



Available online at www.sciencedirect.com

ScienceDirect

journal homepage: www.journals.elsevier.com/oceanologia/



ORIGINAL RESEARCH ARTICLE

Wind wave climate of west Spitsbergen: seasonal variability and extreme events

Kacper Wojtysiak ^{a,*}, Agnieszka Herman ^b, Mateusz Moskalik ^a

^a Institute of Geophysics, Polish Academy of Sciences, Warszawa, Poland

^b Institute of Oceanography, University of Gdańsk, Gdańsk, Poland

Received 28 August 2017; accepted 18 January 2018

Available online 6 February 2018

KEYWORDS

Arctic;
Wave climate;
Hindcast;
Reanalysis;
Svalbard

Summary Waves are the key phenomenon directly influencing coastal morphodynamics. Facing insufficient observations, wind wave climate of the west coast of Spitsbergen can be characterized on the basis of the modelled data. Here we have used the results of spectral wave models: Wave Watch III (WW3) hindcast and WAM in ERA-interim (ERAi) reanalysis. We have observed the presence of seasonal cycle with difference of up to 1 m between significant wave heights in summer and winter. In wave-direction analysis we have noticed the southwestern swell component of remarkably narrow width, thus we expect unidirectional swell impact on the coastline. Extreme events analysis revealed that storms occur mainly in winter, but the most energetic ones (significant wave height of up to 9.5 m) occur in spring and autumn. We have identified positive trends in storms' frequency (2 storms per decade) and storms' total duration (4 days per decade) on the south of the study area. More storms can result in the increase of erosion rate on the southwestern coasts of Spitsbergen, but this change may be highly dependent on the sea ice characteristics. Wave heights of wind sea and swell are correlated with the relevant atmospheric circulation indices, especially the North Atlantic Oscillation. In the recent decade, the correlation is stronger with WW3 than with ERAi data, at some locations explaining over 50% (over 30%) of the total variance of wind sea (swell) wave heights. In ERAi data, the relationship with circulation indices seems sensitive to the length of the analysis period.

© 2018 Institute of Oceanology of the Polish Academy of Sciences. Production and hosting by Elsevier Sp. z o.o. This is an open access article under the CC BY-NC-ND license (<http://creativecommons.org/licenses/by-nc-nd/4.0/>).

* Corresponding author: Institute of Geophysics PAS, ul. Księcia Janusza 64, PL-01-452 Warszawa, Poland. Tel.: +48 601807333.

E-mail addresses: kwojtys@igf.edu.pl (K. Wojtysiak), oceagah@gmail.com (A. Herman), mmosk@igf.edu.pl (M. Moskalik).

Peer review under the responsibility of Institute of Oceanology of the Polish Academy of Sciences.



Production and hosting by Elsevier

<https://doi.org/10.1016/j.oceano.2018.01.002>

0078-3234/© 2018 Institute of Oceanology of the Polish Academy of Sciences. Production and hosting by Elsevier Sp. z o.o. This is an open access article under the CC BY-NC-ND license (<http://creativecommons.org/licenses/by-nc-nd/4.0/>).

1. Introduction

Wind wave conditions are an important feature in variety of coast-related processes (Semedo et al., 2015; Wang and Swail, 2001; Zacharioudaki et al., 2015). Instrumental monitoring of waves is usually restricted to single points (buoys, ships, oil platforms) or relatively narrow areas via remote sensing (regarding small time scales). The downside of those techniques is usually insufficient temporal and/or spatial extent and/or resolution. Recent development of numerical methods (Thomas and Dwarakish, 2015 and the references therein) resulted in the gain of scientific acclaim of modelled data due to its increasing precision. Simulations, unlike measurements, are free from the limitations of purely observational approach.

In this study, we are using model-based hindcast/reanalysis to describe wind-wave characteristics of the north-eastern Greenland Sea shelf area, west of Svalbard Archipelago. In situ wave monitoring is rare in the offshore areas of the Arctic. Several buoys are deployed only in the area of Chukchi Sea and the ones in Atlantic Ocean are located in the area of the western Iceland shelf and north-east of Shetland Islands, several hundreds of kilometres from the area of interest of the present study. Although some observations of the waves are being conducted, location of buoys is restricted to in-shore areas in fjords, in shallow (order of 10–30 m) water, which puts the validation of the model data from off-shore locations in question.

Few papers describe wind waves in regions that contain this study's domain (Reistad et al., 2011; Semedo et al., 2015; Stopa et al., 2016). Moreover, they have larger-scale, regional character, as opposed to this paper, which aims to characterize a relatively small part of the Arctic Ocean's coastal zone.

Wave climate in the study area consists of swell from the North Atlantic and locally generated wind waves, and is influenced by a number of factors including the sea ice coverage, bathymetry, tidal currents. Wave climate of the Nordic-Greenland Seas is characterized by well-marked seasonality of significant wave height (H_s), with stormy period in December through February, followed by a decrease in spring and a calm period in June to mid-August (Stopa et al., 2016).

Apart from seasonal variability, the wave climate undergoes long-term changes. Many studies (e.g. Bertin et al., 2013; Kushnir et al., 1997; Young et al., 2011) indicate the presence of a positive trend in wave heights for the Northern Hemisphere with the emphasis on the North Atlantic. Stopa et al. (2016) conclude that wind speeds and wave heights on Nordic-Greenland Seas have been increasing within the last 20 years, and mention the role of atmospheric indices (e.g., North Atlantic Oscillation) in the process. They also indicate the prevalence of swell in the total wave energy, but the role of sea-ice interactions with waves is unclear. Semedo et al. (2015) also notice a significant share (not less than 50%) of swell in the total significant wave height, and their results indicate prevailing directions of waves origin to be southwest for swell, and east for wind sea, regardless of the season.

This paper focuses on characterizing the west Spitsbergen wave climate on the basis of hindcasted and reanalyzed wave parameters which are: significant wave height (H_s), peak

period (T_p), –1st moment mean period (T_m), and incoming wave direction (Θ). The goal is to describe typical wave conditions and to extract information about occurrence, frequency and duration of extreme events. Our main motivation for conducting this study is that there are, to our knowledge, no similar research studies conducted for this area so far, despite its importance in, e.g., impact on coastal erosion rates. In the study by Zagórski et al. (2015), it is clearly pointed out that wave activity and storm occurrence strongly contribute to erosion rates of the coast of Isbjørnhamna, one of the Hornsund fjord's bays, posing a threat to the infrastructure of the Polish Polar Station located there. In other research, Sessford et al. (2015), analyzed data from field sites located in the inner parts of Isfjorden and Van Mijenfjorden and concluded that the influence of waves on the coasts was minimal. The two examples with seemingly contradictory conclusions actually suggest significant differences in wave influence on individual parts of the coast. Results from local studies cannot be extrapolated to the coasts of the west Spitsbergen in general.

Details on the area of interest, data sources and used methods are described in the next section of this paper, which is followed by the results and discussion on seasonality, wave directions, wind wave extreme events and possible correlations with chosen atmospheric indices. Conclusions and remarks about the future goals are presented in the last section.

2. Data and methods

2.1. Study area

Svalbard is an isolated archipelago influenced climatically by two substantially different water bodies — the Arctic and Atlantic oceans. Spitsbergen, the biggest island of the archipelago, is a vivid example of the above. Its east coast remains under a cold regime of Arctic waters, while the climate of the western shores is significantly altered by the warm North Atlantic Current originating in the Gulfstream (Drange et al., 2005; Przybylak, 2003). Przybylak (2003) points out that the Atlantic region of the Arctic — defined as the combined areas of Greenland Sea, Barents Sea and Svalbard — stands out from its remaining parts, as it is significantly warmer (up to 20°C higher monthly mean air temperature, compared to other regions of the same latitude). Wind speeds in this area are also of the highest in the entire Arctic. Since prevailing winds in the region are Polar Easterlies, main wind directions are from the east and north east, with speeds up to 8–10 m s⁻¹ (monthly average) and directional distribution narrow during winter, while summer months are characterized by wind speeds of ca. 5 m s⁻¹ and the directional distribution is considerably wider.

The seas to the west of Spitsbergen are, in general, free of multiyear ice (Johannessen et al., 2004; Onarheim et al., 2014). In the past 3 decades, first year sea ice developed only in the Sorkapp area in the far south and close to the Albert I Land in the far north. As Onarheim et al. (2014) describe, sea ice extent north of Svalbard gradually decreased in last decades. What has to be mentioned to complete the description of the ice conditions is the

phenomenon of sea ice clusters of considerable ice concentration (>30%), which are episodically observed along the west coast of Spitsbergen. These events are of variable duration (days to months long) and scale. They may occur in late winter throughout spring, up until late autumn, and are very well visible in remote sensing data (<http://polarview.met.no/>). Styszynska and Buchert (2004) have described one of the most prominent events of this kind that took place from May to July 2004, when closed drift ice formed a 50-km-wide stream along the west coast of Spitsbergen, significantly disturbing marine traffic in the area. The scale of the event was explained by a shift of the West Spitsbergen Current (WSC) to the west. This shift, combined with atmospheric circulation at that time, created favourable conditions to move substantial ice masses from the southeast part of the Island to the south-west and further northwest. A similar event of a smaller scale occurred from May to June 2011, and was briefly mentioned by Kruszewski (2012). This kind of sea ice behaviour is observable in the ice coverage data sets used in this paper and may have significant influence on wave propagation from the open ocean to the coasts.

For our study we have chosen the north-eastern part of the Greenland Sea, bordering with the west coast of Spitsbergen. The latitudes of the domain of study span the range between 76 and 80°N, while longitudes are contained within 5 and 20°E (Fig. 1a). For a detailed analysis we selected 9 points along a line that follows the general, approximate shape of the Spitsbergen coastline and its shelf (Fig. 1b), with the purpose to analyze spatial variability of the wave environment in different parts of the domain of interest. All points are located within the shelf area, 15–55 km from the coast and the ocean depth varies between 155 and 380 m with exception of point 3 (80 m) and 9 (490 m).

2.2. The datasets

As a source of wind wave data, two datasets were used. The National Oceanic and Atmospheric Administration's (NOAA) WaveWatch III (WW3) hindcast was obtained from the archive located on public NOAA's Environmental Modeling Center/Marine Modeling & Analysis Branch ftp server (<ftp://polar.ncep.noaa.gov/pub/history/waves>). The second source was the European Centre for Medium-Range Weather Forecasts' ERA-Interim (ERAi) reanalysis (Dee et al., 2011). Both datasets are open-access databases. We decided to use two independent sources based on two different models with some differences in algorithms describing the physical processes, in numerical methods, as well as configuration, particularly in terms of wave frequency cut-off and treatment of the sea ice influence (Dee et al., 2011; Tolman, 2014). WW3 data offers higher spatial and temporal resolution, as well as better performance in terms of swell propagation, while ERAi delivers longer time series which is necessary for an analysis of long-term variability. For the comparison of both datasets' selected characteristics see Table 1.

2.3. WW3

We have acquired nearly ten-year time series (February 2005–March 2015) of H_s , T_p and Θ with temporal resolution of 8 measurements a day, and grid cell size of $0.5 \times 0.5^\circ$. WW3 hindcast, apart from bulk parameters characterizing whole wave energy spectra, contains also data derived from 2-dimensional energy spectra separated into variable number of partitions, which enables analysis of separate wave systems aside from their superposition. These data were used in the analysis of wave directions. Full documentation of the WW3 model can be found in WaveWatch 3 manual by Tolman (2014). As an additional variable, sea ice concentration

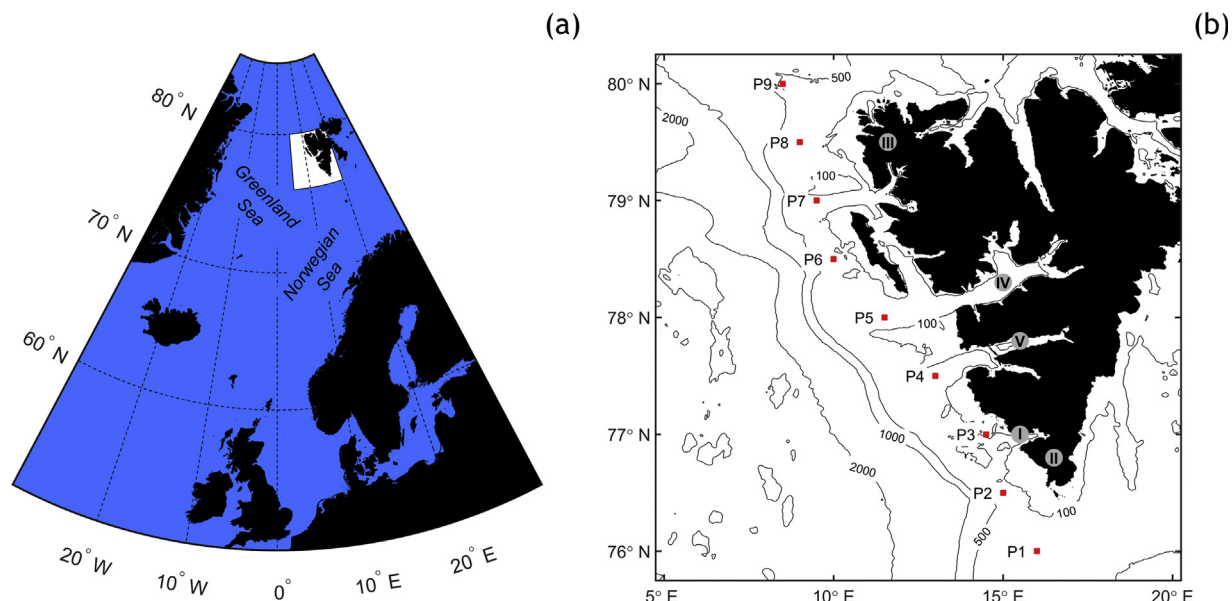


Figure 1 (a) Map of North Atlantic with the study area shown as white field. (b) Grid limits of the study area with points of analysis marked red and numbered from P1 to P9. Grey circles mark the locations as follows: I – Polish Polar Station in Hornsund, II – Sorkapp, III – Albert I Land, IV – Isfjorden, V – Van Mijenfjorden.

Table 1 Comparison of the datasets used in the analysis.

	WW3	ERAi
Spectral wave model used	WaveWatch III	WAM
Partitioning of energy spectra	Bulk, wind sea, up to 9 swells	Bulk, wind sea, total swell
Dataset time range used	Feb 2005–Apr 2015	Jan 1979–Dec 2015
Native spatial resolution [°]	0.5 × 0.5	1 × 1
Temporal resolution (values per 24 h)	8	4
Spectral resolution	36 directions 50 frequencies	24 directions 30 frequencies

values were obtained from the NCEP/NCAR Climate Data Assimilation System (<ftp://polar.ncep.noaa.gov/pub/cdas/>). Ice concentration data is available in the same spatial resolution, but calculated once per day.

2.4. ERAi

ERAi wind wave data is based on the modified WAM model, improved in terms of parameterization of physical processes important for long-term, climate simulations. The model is two-way coupled to the atmospheric model and its operational resolution is 1 × 1°. Time series of H_s , T_m and Θ were extracted for period from January 1979 to December 2015 with temporal resolution of 4 measurements per day. The data was retrieved as bulk, and also as two separate partitions of wind sea and total swell. ECMWF database offers the option to linearly interpolate grid data for selected parameters. Option 0.5 × 0.5° was chosen to obtain data at the same locations as the WW3 hindcast. No temporal interpolation was applied to the timeseries. ERAi archive delivers also sea ice concentration data, which were, additionally, extracted in the same spatial and temporal resolution as the wave data. For further information about ERAi reanalysis and WAM model configuration, see [Dee et al. \(2011\)](#) and references therein.

2.5. Data processing

The time series extracted from both data sets were inspected for continuity, and multiple fragments containing 'not-a-number' values (NaNs) in the ERAi and WW3 data were found. These NaNs are related to the models' configuration: wave energy is set to zero in grid points in which sea ice concentration exceeds a limiting value, equal to 0.30 in ERAi and 0.67 in WW3 (for ice concentrations between 0.33 and 0.67, WW3 uses a parameterization of wave propagation and attenuation in ice). The amount of NaNs in ERAi time series is therefore significantly higher than in WW3. To summarize, in majority of cases 'NaNs' in the data represent grid masking related to the presence of sea ice. All analyses in this study are performed using the standard type I (Ice time included) strategy that is thoroughly explained by [Tuomi et al. \(2011\)](#).

Before proceeding with further analysis, we compared the modelled H_s values with the available observation data ([Fig. 2a, b](#)). Additionally, a comparison of the WW3 and ERAi datasets was performed (see below and Supplementary Note S1). The next step was calculating seasonal variability of significant wave height for both sets in their full time range.

Here, apart from calculating the daily mean H_s values, LOESS model was applied to generate smoothed curves for both mean and 99th percentile values. Next, diagrams of daily mean H_s values were created for each point.

Due to the fact that initial study of period time series did not show clear seasonal pattern, and that both datasets contain different type of wave period data (peak period in WW3 and mean period in ERAi); period related analysis was not included in the main text. Instead, it is illustrated in the supplementary material (see Supplementary Note S1 and Supplementary Fig. S5).

For visualization of incoming wave directions, the partitioned WW3 data were used, with separated wind wave and a number of swell fractions. WW3 data are divided into partitions corresponding to modelled wave systems. Each partition is assigned a wind fraction parameter, ranging from 0 (swell wave) to 1 (wind sea). In order to eliminate from further analysis partitions of uncertain type, entries with wind fraction values between 0.3 and 0.7, which make circa 5% of the data, were not considered in calculations. For details on WW3 partitioning scheme and wind fraction calculation see [Tolman \(2014\)](#), section 3.9.

For analysis of extreme events we applied automated approach to obtain local H_s maximum values. Matlab function – *findpeaks* was used to extract the subset of peak values (H_s) with their location (in time) and width (duration) in the timeseries. In order to configure the function properly, we used elements of Peaks Over Threshold method – a statistical approach that involves the analysis of the sample of independent extreme values over a certain threshold ([Teena et al., 2012](#)). The function was given the following arguments:

- Minimum peak height (h_{mp}), restricting the algorithm to ignore peaks lower than the given value, expressed in metres; an analogue of the threshold value in the POT method,
- Minimum peak prominence (p_{mp}), a difference between considered peak and the local minima with relation to the peaks in the neighbourhood, expressed in metres; *findpeaks* will ignore small peaks on the slopes of the tall ranges of major peaks, but will preserve isolated peaks of given prominence, if all other conditions are met,
- Minimum distance between peaks (d_{mp}), expressed in hours, forces the algorithm to find peaks outside the specified range of each other; a declustering routine to prevent identifying groups of clustered peaks as separate events.

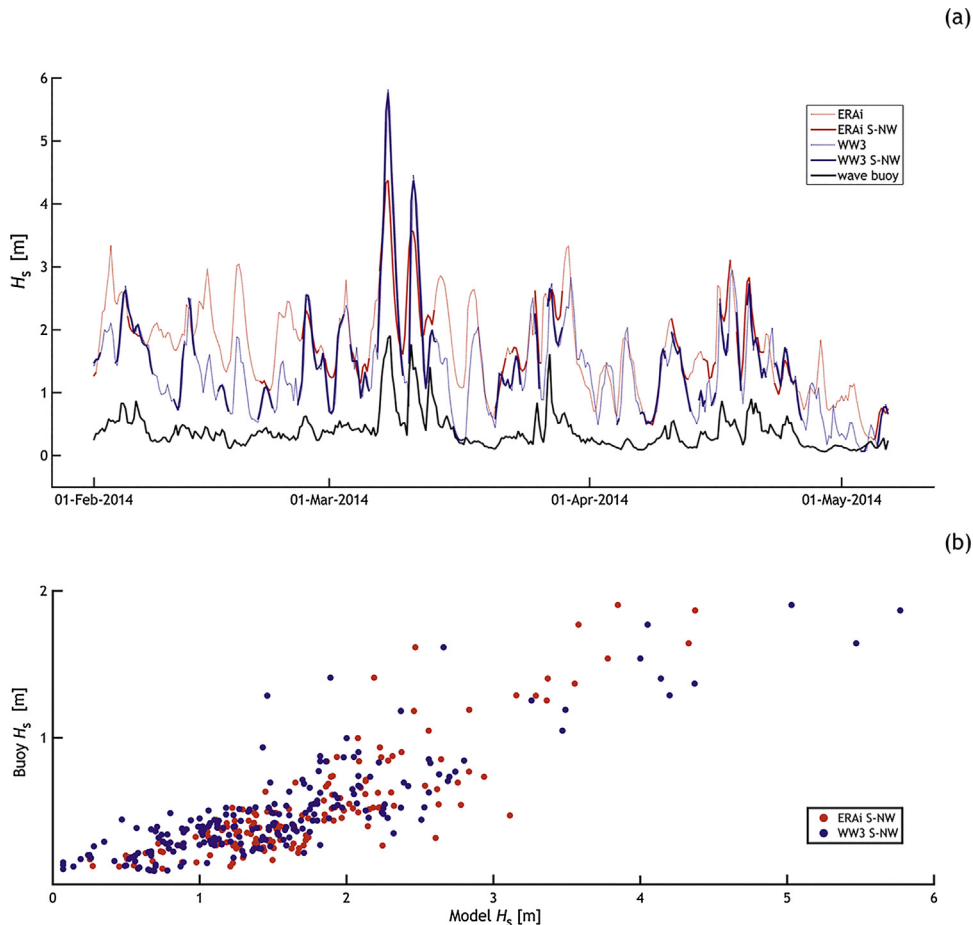


Figure 2 (a) Comparison of H_s time series from wave products used in this study (point P3 in Fig. 1b) with the wave buoy data from in-shore location in Hornsund fjord (marked “I” in Fig. 1b). The sections of the modelled time series with wave directions propagating from the directions (Θ) between 180° (South) and 300° (North-West) are marked with thick lines. (b) Scatterplot of modelled H_s associated with Θ in range of 180–300° against the wave buoy data.

With the above arguments introduced, the algorithm scans the time series finding the highest peak, discards all peaks in range of d_{mp} , then repeats until there are no more peaks to consider.

The h_{mp} argument was initially set to 2.5 m – a value that corresponds to the 90th percentile of all WW3 and ERAi H_s values from all points combined. This approach enabled the analysis of extremes with the reference of the entire study area. After visual inspection of H_s time series, by the method of trial and error the p_{mp} value was set to 1 m to prevent finding low and/or short peaks. The d_{mp} value was deduced from iterative test, when the argument was inputted in range from 6 to 360 h and compared against the resulting number of peaks found by the function. After exceeding 24 h the number of peaks retrieved decreases rapidly while the mean time between two consecutive peaks started to increase from the base level of approximately 48 h. Regarding the fact that the average storm duration is shorter than the average time between the two consecutive storms, we set the d_{mp} to 72 h which is a sum of the average storm duration and the shortest period of silence directly after it. We have found this value high enough to consider all resulting peaks independent, but low enough to avoid sacrificing

the size of the final subset by excluding consecutive yet independent events.

In order to elucidate the influence of the large-scale atmospheric forcing on wave conditions in the region of interest, we analyzed linear correlation coefficients between the wave height (for wind sea and swell separately) and atmospheric circulation indices associated with those Northern Hemisphere teleconnection patterns that exhibit strong activity over the North Atlantic and parts of the Arctic surrounding the Svalbard Archipelago. The climate teleconnection data are available from the Climate Prediction Center of the U.S. National Weather Service (<http://www.cpc.ncep.noaa.gov/data/teledoc/telecontents.shtml>). The patterns and their associated indices are obtained with a Rotated Principal Component Analysis (RPCA) applied to standardized (by monthly means and standard deviations) height anomalies of the 500 hPa isobaric surface heights north of 20°N, starting from January 1950. In our analysis, we use monthly indices of the following five patterns: North Atlantic Oscillation (NAO), East Atlantic (EA), East Atlantic/Western Russia (EAWR), Polar/Eurasia (POLEUR) and Scandinavia (SCAND). Due to their calculation procedure, the indices are linearly uncorrelated (e.g., in the subset of the

whole dataset corresponding to the WW3 time frame, i.e. 2005–2015, all absolute values of the pairwise correlation coefficients are lower than 0.08, see Suppl. Fig. S1). Additionally, we use time series of the monthly Arctic Oscillation (AO), the leading mode of variability of the anomalies of the 1000 hPa isobaric surface heights poleward of 20°N, as AO is routinely used in climate studies in the Arctic. Because the 500 and 1000 hPa anomalies are not independent (especially over the North Atlantic, where both are dominated by the Icelandic low and the Azores high), there is a strong correlation between the leading modes of their variability. In the period 2005–2015, the correlation coefficient between AO and NAO equals 0.63; AO is also significantly correlated with SCAND (−0.24) and POLEUR (0.24), see Suppl. Fig. S1. For ERAi data, the correlation coefficients with the atmospheric circulation indices were calculated for two time periods: 2005–2015 (to compare with analogous values for WW3 data) and 1979–2015.

2.6. Data reliability and consistency

Both data sources used in this study have certain limitations regarding the expected accuracy of the data. Firstly, the spatial resolution of both models was too low to depict the study area's shoreline and bottom topography with sufficient detail. Secondly, the spatial resolution of the wind data used to force the wave models was too low to describe details of Svalbard's landscape. Therefore, it is reasonable to expect lower accuracy of the wave products for short-fetched waves generated locally by easterly winds (which is the dominating wind direction in the analyzed region).

As already mentioned in the introduction, all available in situ wave measurements in the area of study are from shallow, in-shore locations, and using these measurements for direct validation of the modelled data from WW3 or ERAi cannot be considered without some important remarks. Fig. 2a illustrates the comparison of the WW3 and ERAi H_s values from point P3 of the analysis to the time series from a pressure sensor based on a wave buoy that was deployed for 100 days in Hansbukta, a bay near the Polish Polar Station in Hornsund, at the depth of 25 m. The location of peaks and the general shape of the curves represent surprisingly good level of similarity (Pearson's correlation coefficients are 0.75 for WW3 and 0.67 for ERAi), particularly when one considers landward wave propagation directions (coeff. of 0.89 for WW3 and 0.86 for ERAi), it is not the case for the rest of the plot. Clearly, both models generate peaks that are absent in the buoy's log; presumably due to the coastline's shape preventing waves of certain directions from propagating into the buoy's location, or due to the increased fetch for seaward winds. The scatterplot of modelled H_s associated with the landward Θ values against the H_s from observations (Fig. 2b) reveals strong linear relationships between the models and the buoy. The last remark is that the H_s values from the buoy are significantly lower than the modelled H_s . Considering the distance and significant decrease in water depth between modelled and monitored location, which results in the transformation of waves entering the fjord, the accuracy of modelled H_s can be described as sufficient for the purpose of this study, with all the remarks mentioned.

Both WW3 and WAM have been evaluated in other studies. Chawla et al. (2013) have validated WW3 model for quality and precision, and concluded that the model performs accurately in the case of the offshore areas, and that there is some decrease in level of agreement for coastal areas, caused by unresolved bathymetric features, and problems with quality of wind input at land margins. Kumar and Naseef (2015) assessed the performance of ERAi wave data in India's nearshore waters and came to similar conclusions; they also found a tendency to overestimate low, and underestimate high H_s values. Stopa and Cheung (2014) have compared wind and wave data from ERAi dataset with NCEP Climate Forecast System Reanalysis (CFSR-W which is based on WW3 model) validating both reanalyses with the same set of altimeter and buoy data, and found that while CFSR-W offers better quality of upper percentile waves, ERAi is more reliable for modelling long-term variability, due to the better temporal homogeneity.

In order to better investigate the quality of the WW3 and ERAi data sets in our area of study, we performed a comparative analysis of these data, complemented with a comparison to a third, local wave product available only within a short period of time. Details of this analysis and its results are presented in the Supplementary Note S1. As can be seen, the overall agreement between the data sets considered is satisfactory, with high correlation coefficients between the respective variables, no significant bias, but relatively high standard deviation of differences (especially in the case of wave directions). Notably, the differences between the models are higher for swell waves (in particular, very-low-frequency swell) than for wind sea. Importantly, even considering errors that inevitably are present in the data, our analyses indicate that the conclusions formulated further in this study are not substantially affected by these errors.

3. Results and discussion

3.1. Seasonality

Most apparent feature of the analyzed data is clear seasonality present in both datasets (Fig. 3). For WW3 the maxima of the mean H_s and the 99th percentile occur between December and January. Their values are 2.6 m and 5.4 m, respectively. For ERAi the general patterns are similar, but the values are higher, with the respective maxima of 2.8 and 6.3 m. This result is consistent with previous studies (Atkinson, 2005; Semedo et al., 2015; Stopa et al., 2016). Additionally, 99th percentile curves modelled with LOESS are less symmetric than the mean H_s , as the descending slopes are steeper than the increasing ones, which implies difference in duration of the transition periods. Moreover, the smoothed curves do not reflect some details that are visible in the daily 99th percentile data (Fig. 3, dotted lines), where maximum values occur in March and therefore the 'high-energy period' ends abruptly in the spring, while the summer–autumn transition is more gradual. Going further, the highest spike of the 99th percentile H_s in the spring corresponds to the vernal equinox (March 20–21st), while the autumn maximum is located near October 30th which is the beginning of polar night for the latitudes considered. In Fig. 4, an approach to visualize inter-annual variability of H_s was made. Seasons are

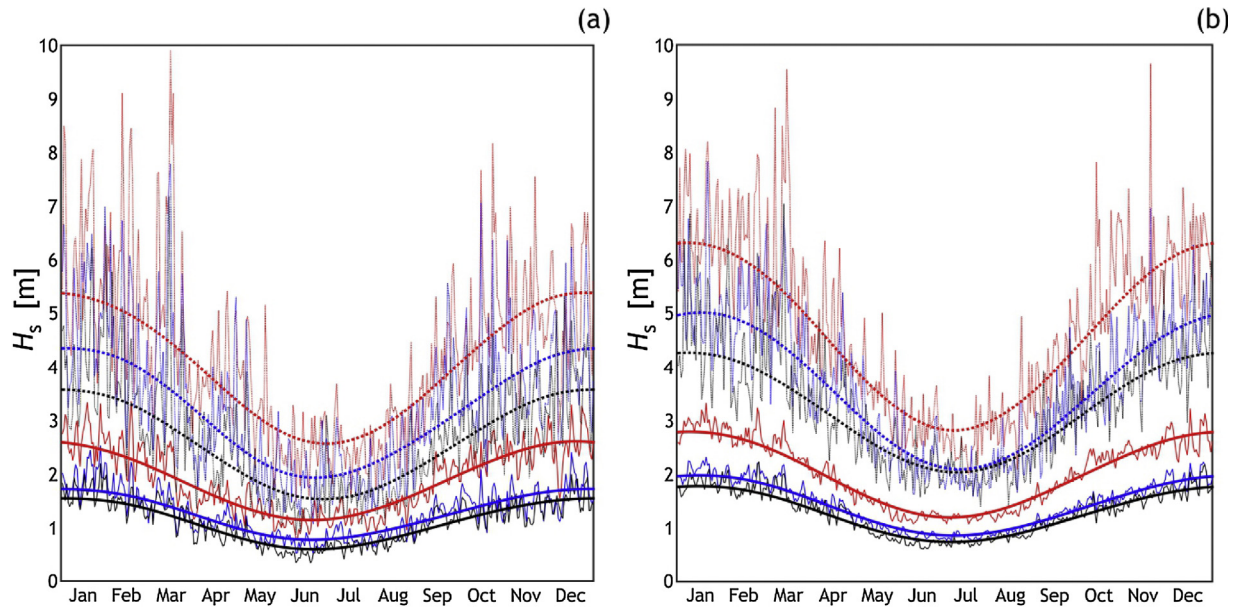


Figure 3 Seasonal variability of H_s in points 1 (red), 5 (blue) and 9 (black) for (a) 10 year period (WW3) and (b) 37 year period (ERAi). Daily means (solid) and 99th percentile (dotted) values are shown. Smoothed lines represent wrapped robust LOESS model.

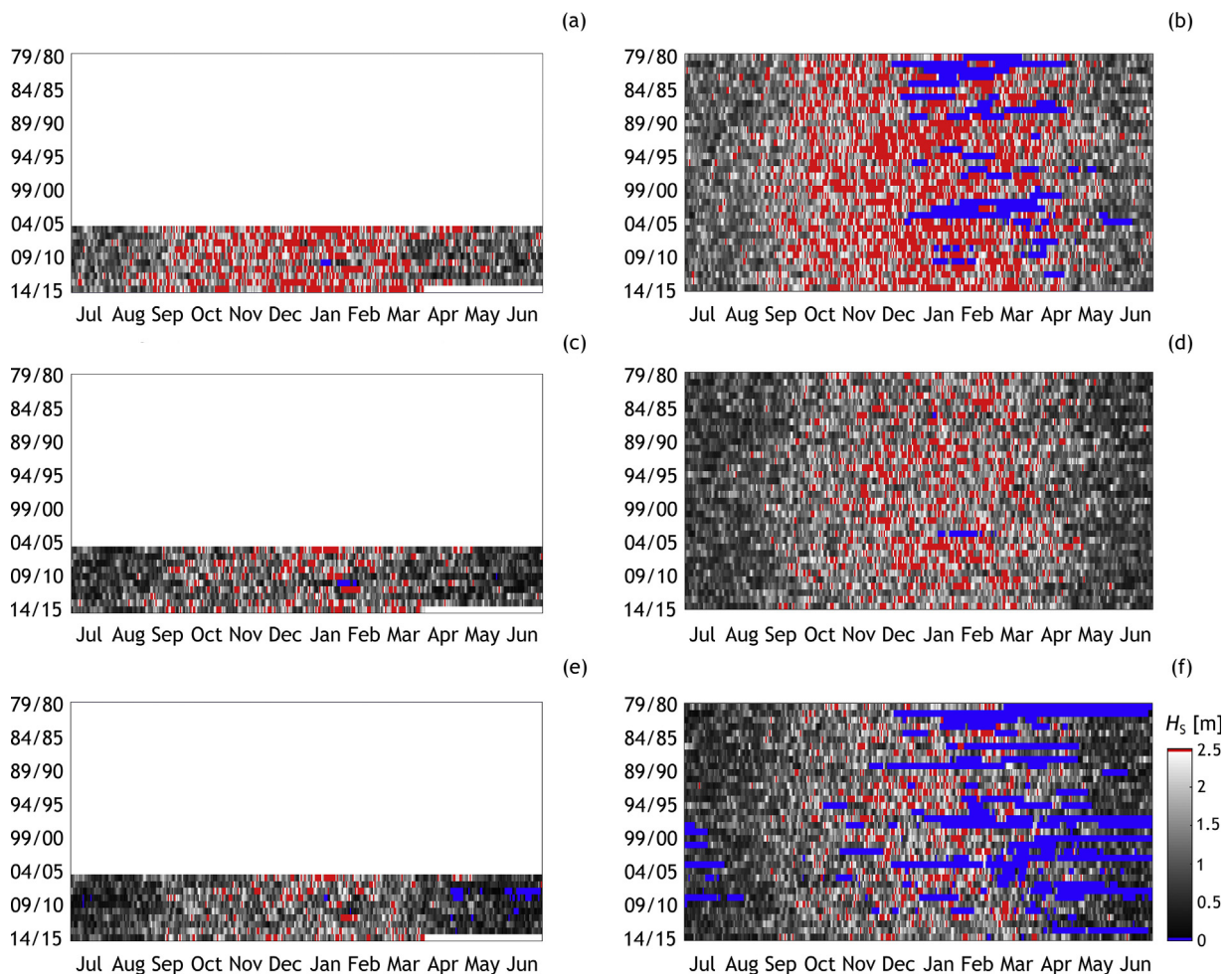


Figure 4 Inter-annual H_s changes in points P1 (a, b), P5 (c, d), P9 (e, f) for WW3 (a, c, e) and ERAi (b, d, f). Each row in the graphic represents single winter-centred season. Blue colour marks the lack of data (sea ice present).

displayed in a 'winter-centred' manner, as it is the part of the year that is most active in terms of wave heights. The graphic confirms seasonal pattern of H_s changes from Fig. 3, but it also shows the extreme event frequency changes during the analyzed periods (red pixels) which is helpful in further analysis of extremes. Also, the sea ice presence can be observed only on southern and northern points of study area.

3.2. Wave directions

It has been recognized that separate analysis of wind sea and swell provides better insight into wave characteristics (Guedes Soares, 1984; Portilla et al., 2009). The visualization of the incoming wave directions (Fig. 5) has been generated from WW3 partitioned data, as we have chosen independent wave systems analysis, where partition-corresponding directions are present instead of mean values calculated from total energy spectra (see Tolman, 2014). These data are not available in ERAi dataset, which offers the data divided to wind sea and swell partitions only. We believe that WW3 approach presents better resemblance to the real-life

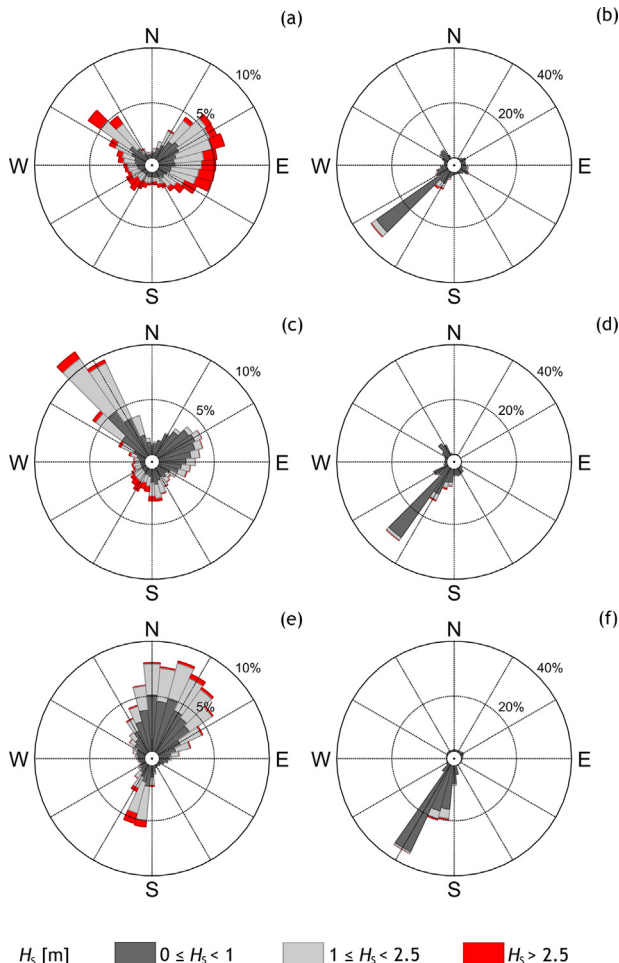


Figure 5 WW3 incoming directions of wind sea (a, c, e) and swell (b, d, f) partitioned components for points P1 (a, b), P5 (c, d) and P9 (e, f). Please note that the scale varies between the wind sea and swell. All directions are presented in meteorological convention. Generated with WindRose code (Pereira, 2014).

situation, than analysing bulk, or separated wind sea and total swell components. Data is presented in form of wave roses with 36 directional bins of 10° width. The results reveal that substantial amount of swell arrives from the south-west with a gradual shift to the south with increasing latitude. Wind sea behaviour is more complex, and prevailing directions, usually two or three, change significantly depending on the analyzed location. At the southern points (P1, P2), the prevailing directions are E and NW. In the middle zone (points P3–P7) waves come mostly from NW, SW and NE, and in the north (points P8, P9) waves from N and NE are the most frequent. These wave directions are in accordance with the wind pattern characterizing the study area presented by Cisek et al. (2017). As mentioned in 'Data reliability and consistency' subsection, wind sea parameters for waves coming from the land directions may be inaccurate, but this is not the case for swell, where incoming directions indicate origin of the majority of waves to be the Norwegian Sea. Point data analysis also suggests that wave activity is more intense in the southern part of the study area which could be related to increase of sea ice concentration while heading north, but in fact, observations of sea ice presence (Norwegian Ice Service – MET Norway: <http://polarview.met.no/>) in the study area show that the problem is more complex, as ice is usually absent in the middle part of the coastline (points P4 to P7) and is mostly present in points P1 to P3 and P9 (see Fig. 4). Therefore we infer that distance from swell generation area is responsible for average swell state, and ice presence distorts this pattern to some degree. Directions of waves and spatial distribution of wave height indicate that the northern parts of the fjords' shorelines, especially in the south of Spitsbergen, are more exposed to wave-driven erosion, which is in accordance to the study of Zagórski et al. (2015). In the case of the west coast of Spitsbergen outside of fjords and bays, effects of sheltering can be omitted as there are no major obstacles for waves further offshore. Bottom morphology influence, on the other hand, is hard to estimate, and demands small scale, local studies.

3.3. Extreme events

Characteristics of extreme events are shown in form of multiplots containing 3 computed variables averaged annually (Fig. 6a, c, e), and seasonally for winter (December, January, February – DJF, Fig. 6b, d, f). Those variables are: annual or seasonal mean of maximum H_s in individual extreme events, denoted with $H_{s,\max}$; extreme events count; and extreme events total duration expressed in days. Analogous plots for spring (March, April, May – MAM), summer (June, July, August – JJA), and autumn (September, October, November – SON), as well as those for WW3 data are available in the Supplementary Material (Suppl. Figs. S9 and S10). For an additional analysis, a parameter describing the number of days with sea ice concentration exceeding 25% has been added. $H_{s,\max}$ values oscillate around 3.5–4 m and lower values are observed in northern locations regardless of the analyzed period. In both datasets the number of extreme events ranges from less than 10 to over 40 annually. Events' total duration spans from 20 to over 80 days per year. In the same time, 25% ice concentration days vary greatly from 0 to 100, and even exceeding 250 in point 9 for ERAi

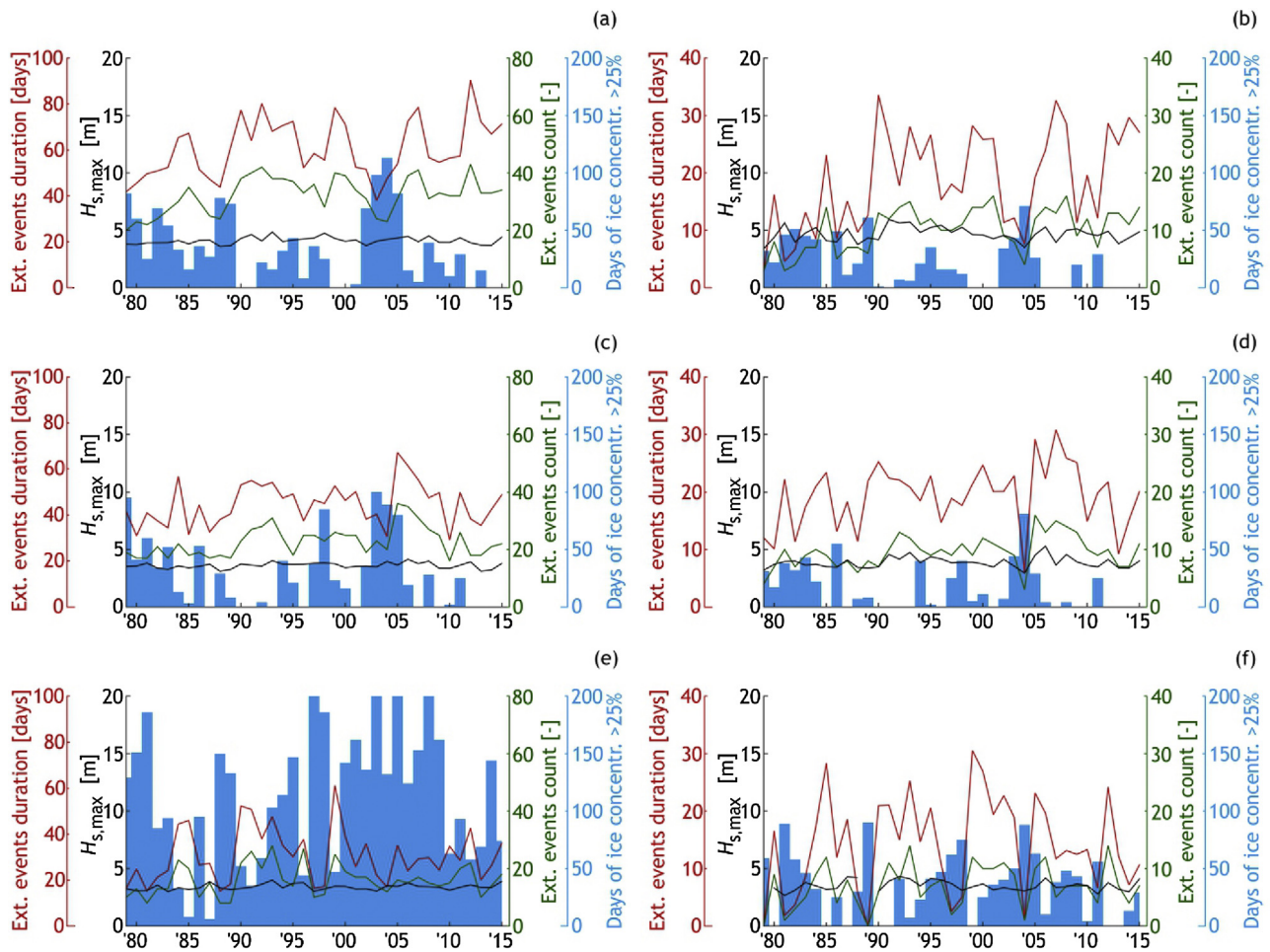


Figure 6 Extreme event parameters calculated from ERAi dataset for annual (a, c, e) and DJF (b, d, f) for points P1 (a, b), P5 (c, d) and P9 (e, f). For practical reasons, instead of being normalized, individual variables have separate y-axes to enable easy absolute value readout. Please note that the scales differ between annual and DJF charts. Generated with addaxis code ([Lee, 2005](#)).

dataset. Examination of $H_{s,\max}$ reveals no significant trend, which can indicate that average extreme events' H_s does not change noticeably in the given time period. This is expected, as $H_{s,\max}$ represents only the scale of the events occurring in given environment, and does not provide the complete information about the events. Information about extreme event count and duration provides a valuable insight about the change of how frequently high sea state occurs in the area and how long it typically lasts. These values vary annually and the WW3 dataset (see Suppl. Fig. S9) is not long enough to observe any trends. However, in 37-year period (Suppl. Fig. S10), the trend in events duration is clear for points 1 and 2. To approximate the trend values, linear regression was performed with a bootstrap method (number of repetitions: 1000), and corresponding values of the mean trend at points 1 and 2 are 0.39 and 0.41 days per year with standard deviation of 0.16 and 0.13, respectively (see Table 2), which gives roughly 9–10 h more of high sea per year. Event count trends (0.23 and 0.20 events per year, both with standard deviation of 0.08) reflect the trend pattern of events duration described above. We infer that the observed trends are not driven by temporal inhomogeneity in the data, as they do not occur uniformly in space, but are restricted to the southern part of the study area only. It seems reasonable to assume

that any temporal inhomogeneities in the data related, e.g., to changes of the model configuration or input data sources would manifest themselves consistently at all analyzed locations instead of producing a spurious signal at some points without affecting neighbouring ones. After analysing the relation between the events count and duration it becomes evident that event count is the key variable, and its increase in time determines the trend of the events' total duration. Remarkably, almost all statistically significant trend values are contained in DJF period. The described differences in wave climate between south and north of the study area correspond to the conclusions by Cisek et al. (2017), who found evidence for southern Spitsbergen being under stronger ocean influence than the north-west.

Ice concentration bar graph was added to extreme event parameters plot to show the substantial influence of sea ice in ERAi data, as drops in the number and duration of extreme events overlap with spikes of the number of >25% ice concentration days. The scale of influence of the short-lived sea ice patches on waves is not well known, but its existence is unquestionable. Its magnitude is determined not only by spatial characteristics of the ice patch itself (its spatial extent, ice type, etc.), but also by wave parameters, as wind sea's expected response will be more

Table 2 Mean slope coefficients and standard deviations of bootstrapped linear trends calculated for annual and seasonal extreme event duration. Significant trends (positive with more than 95% probability) are shown in bold.

Point no.	Annual		DJF		MAM		JJA		SON	
	Trend [d y ⁻¹]	Std. dev.								
1	0.39	0.16	0.38	0.11	0.05	0.11	-0.04	0.06	0.03	0.04
2	0.41	0.13	0.37	0.10	0.06	0.09	-0.04	0.04	0.06	0.06
3	0.07	0.17	0.11	0.12	-0.04	0.08	-0.02	0.03	0.06	0.05
4	0.10	0.16	0.13	0.12	-0.07	0.07	-0.02	0.02	0.11	0.07
5	0.16	0.14	0.10	0.09	-0.01	0.06	0.00	0.02	0.10	0.07
6	0.11	0.16	0.08	0.10	0.00	0.08	0.01	0.04	0.06	0.05
7	0.23	0.15	0.16	0.10	0.03	0.07	-0.01	0.02	0.07	0.07
8	0.12	0.15	0.13	0.10	-0.02	0.06	-0.01	0.02	0.04	0.05
9	0.04	0.16	0.08	0.12	0.03	0.06	-0.02	0.02	-0.05	0.04

noticeable than the response of swell, which can propagate within the ice over great distances (Ardhuin et al., 2016; Zhao et al., 2015).

3.4. Correlation with atmospheric indices

The correlation coefficients between the atmospheric circulation indices and significant wave height of wind sea and swell at points 1–9 are shown in Fig. 7. For the ERAi data, they are calculated in two versions, for the “WW3 time period” 2005–2015 and for the whole period 1979–2015.

In the 2005–2015 decade, the overall pattern of the values of the correlation coefficients is relatively uniform along the whole west coast of Spitsbergen, especially in the case of swell (Fig. 7b, d), which predominantly travels from the open ocean and is not sensitive to local conditions at individual points. As expected, the point-to-point variability is higher in the case of wind sea, strongly affected by the neighbouring coastline. This is the case especially for the WW3 data (Fig. 7a).

At all points, the highest positive correlation is obtained for NAO, in the case of WW3 exceeding 0.4 for H_s of swell and at some points reaching 0.5 for H_s of wind sea. This significant correlation with NAO is not surprising, as a number of earlier studies demonstrated significant influence of this pattern on various local atmospheric, oceanic and glacial processes in Svalbard, including the length of the melting season (Kvamstø et al., 2011), hydrography of the West Spitsbergen Current (Saloranta and Haugan, 2001), or changes in air temperature and precipitation (Osuch and Wawrzyniak, 2016). As the archipelago is located to the north-east of the centre of the Icelandic low, it experiences stronger than usual winds from the southerly sector during positive phases of NAO, i.e., from directions favourable to wave development. The same is true for AO, itself related to NAO (see section on data processing), although the respective correlations are weaker. In the case of wind sea, comparable correlations are observed at central points (No. 3–5) for the POLEUR pattern, in its positive phase associated with negative pressure anomalies over the central Arctic, and with a strong circumpolar vortex. Correlation of similar strength to that with NAO, but opposite in sign, occurs between wind sea and EA, the second most prominent pattern over the North Atlantic region, associated with an extensive

low-pressure system south of Island and north of the Azores (a so-called “southern-shifted NAO”). In the analysis period 2005–2015, EA stayed almost exclusively in its positive phase; in particular, it never dropped below zero after February 2012. Due to the above-mentioned southerly shift of the EA centre relative to the centre of NAO, EA tends to be associated with easterly rather than southerly winds, which explains the negative correlation with wind sea west of Svalbard and very low (0.1–0.2) correlation coefficients with swell. The relationships of wave heights with the remaining indices are lower, although in the case of WW3 data many are statistically significant. Overall, the five uncorrelated indices together explain 30–35% of the total variance of H_s of swell (except at point 9) and between 9 and 68% of variance of H_s of wind sea at the analyzed locations (Fig. 8). Remarkably, whereas the correlation coefficients for swell in the period 2005–2015 are almost the same in ERAi and WW3 (read and blue curves in Fig. 8b), this is not the case for wind sea, where correlations with WW3 are significantly higher, with higher point-to-point variability (Fig. 8a). This may be a consequence of higher spatial resolution of WW3 data that enables better representation of locally generated wind waves. The values of the correlation coefficients with ERAi data are not only lower and more spatially uniform – they are also substantially lower for the period 1979–2015 than for 2005–2015 (Figs. 7e, f and 8). A possible explanations is that either the ERAi data or the atmospheric data used to calculate the atmospheric circulation indices (or both datasets) are non-uniform within the years 1979–2015. Another one is that, at least for some circulation patterns, the period 2005–2015 is too short to cover their whole range of variability (see, e.g., the comment on the EA pattern above, that hardly went into its negative phase since 2012), which may lead to some spurious correlations not present when longer time periods are considered. The above explanations are not mutually exclusive, and their relevance is impossible to determine based on the information available.

4. Conclusions

This study described wind wave climate of West Spitsbergen based on two independent model datasets covering 10 and

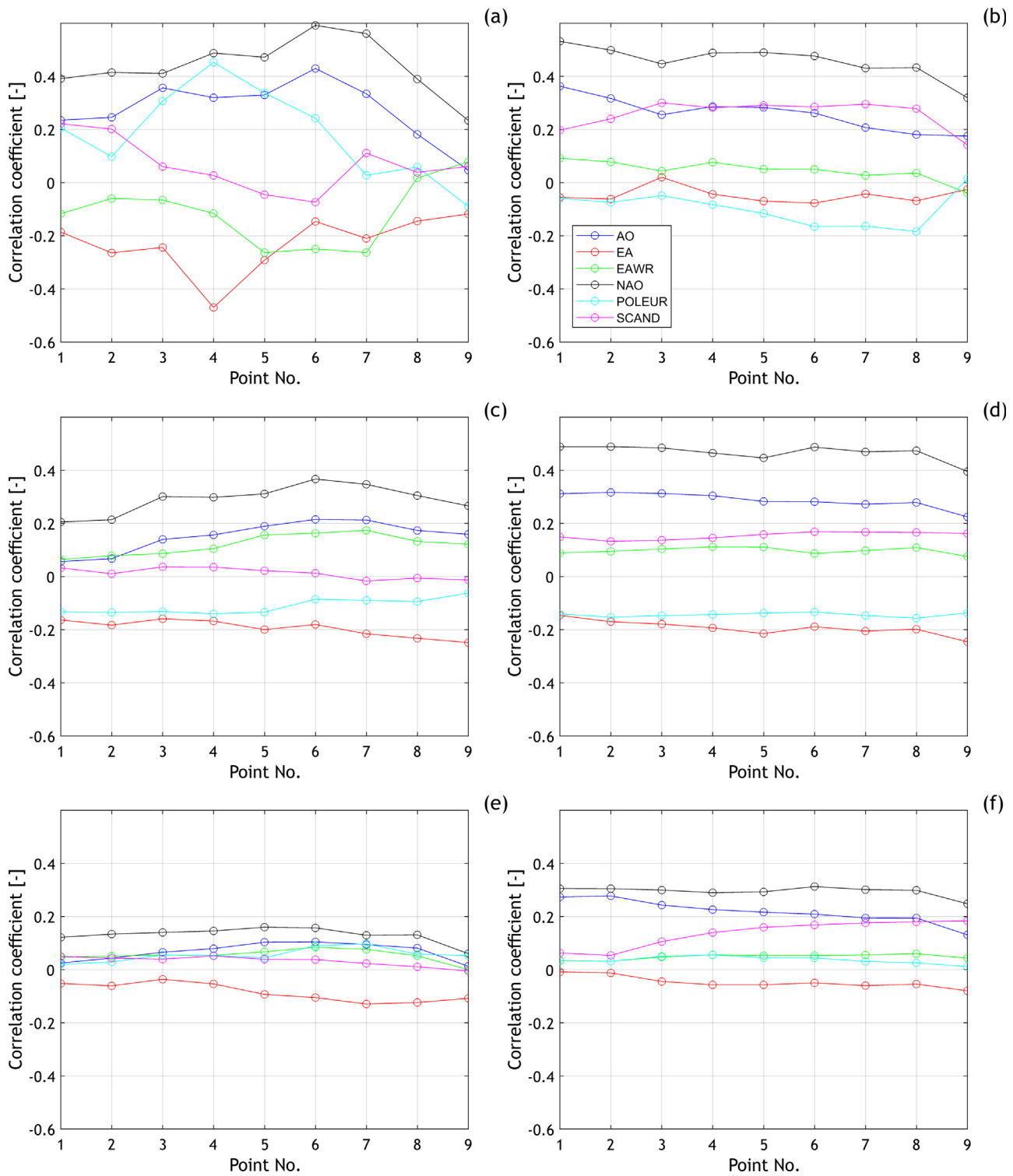


Figure 7 Correlation coefficients between the atmospheric circulation indices and the significant wave height of wind sea (a, c, e) and swell (b, d, f) in the nine analyzed points, calculated for the WW3 data in the period 2005–2015 (a, b), and for the ERAi data in the period 2005–2015 (c, d) and 1979–2015 (e, f).

37-year time period, respectively. Wave data from 9 offshore locations were analyzed to establish short and long-term characteristics of the wave environment at its typical and extreme states.

Seasonal pattern of wave heights in the investigated area resembles the North Atlantic annual cycle, with northward-decreasing differences between winter and summer. As expected, high-sea-states are most frequent in winter, but

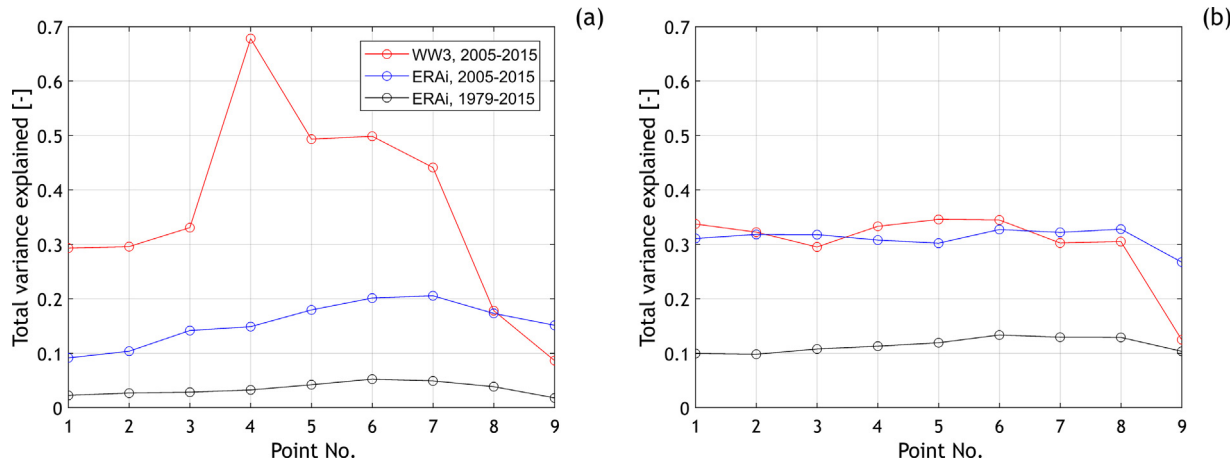


Figure 8 Fraction of the total variance of the WW3 and ERAi wind wave (a) and swell (b) wave height explained by the 5 independent atmospheric circulation indices (EA, EAWR, NAO, POLEUR and SCAND) at points P1–P9.

the highest 99th percentile wave height values coincide with the early spring and late autumn.

Wave direction characteristics have been based on WW3 multi-partitioned data. The general wind sea direction is from the north-west, with exception of points located farthest to the south and farthest to the north, where, respectively, easterly and northerly waves are significant part of the spectrum. The pattern of swell component is unequivocal with over 60% of swell direction values in the data is southwest. This pattern clearly indicates unidirectional swell conditions on entrances to all West Spitsbergen fjords, which may result in easily predictable swell component influence on coastal morphodynamics.

On the basis of extreme event analysis conducted in this study we conclude that among the components constituting extreme events, frequency is the key variable that visibly increased for the last four decades, which is expressed in the positive trends of extreme events count and their total duration. Positive trends have been found to be of the most statistical significance in the south part of the study area, and exclusively during the winter. Interestingly, ice conditions in the southern part of study area are more stable than in the north, which would suggest, that ice regime is not connected to the extreme events frequency trend by means of local influence, however we cannot exclude diminishing sea ice as an indirect cause affecting the waves through impacting atmospheric circulation on regional scale. Nevertheless, it has to be stressed that the sea ice impacts wave climate, and the topic of sea-ice and waves' mutual dependencies demands further investigation.

Association of NAO index to H_s values on West Spitsbergen is significant, but somewhat problematic, as it varies in time and is much stronger for the period of last 10 years, than for the period 1979–2015. There are at least two possible reasons to explain this result, but despite the fact, that ERAi database is generally acclaimed for good quality in terms of data integrity, further study on this issue is necessary to properly address it.

Acknowledgements

This work has been financed by National Science Centre project no. 2013/09/B/ST10/04141. This work was also

partially supported within statutory activities no. 3841/E-41/S/2016, 3841/E-41/S/2017 of the Ministry of Science and Higher Education of Poland, and from the funds of the Leading National Research Centre (KNOW) received by the Centre for Polar Studies for the period 2014–2018.

We would like to thank the two Anonymous Reviewers for their helpful remarks. We would also like to thank Brandy Bell for her swift and selfless input in the language proofreading.

All wind wave products used in this paper were provided by National Oceanic and Atmospheric Administration (NOAA) and European Centre for Medium-Range Weather Forecasts (ECMWF), and are publicly available.

Appendix A. Supplementary data

Supplementary data associated with this article can be found, in the online version, at doi:[10.1016/j.oceano.2018.01.002](https://doi.org/10.1016/j.oceano.2018.01.002).

References

- Ardhuin, F., Sutherland, P., Doble, M., Wadhams, P., 2016. Ocean waves across the Arctic: attenuation due to dissipation dominates over scattering for periods longer than 19 s: observed ocean wave attenuation across the arctic. *Geophys. Res. Lett.* 43 (11), 5775–5783, <http://dx.doi.org/10.1002/2016GL068204>.
- Atkinson, D.E., 2005. Observed storminess patterns and trends in the circum-Arctic coastal regime. *Geo-Mar. Lett.* 25 (2–3), 98–109, <http://dx.doi.org/10.1007/s00367-004-0191-0>.
- Bertin, X., Prouteau, E., Letetrel, C., 2013. A significant increase in wave height in the North Atlantic Ocean over the 20th century. *Glob. Planet. Change* 106, 77–83, <http://dx.doi.org/10.1016/j.gloplacha.2013.03.009>.
- Chawla, A., Spindler, D.M., Tolman, H.L., 2013. Validation of a thirty year wave hindcast using the Climate Forecast System Reanalysis winds. *Ocean Model.* 70, 189–206, <http://dx.doi.org/10.1016/j.ocemod.2012.07.005>.
- Cisek, M., Makuch, P., Petelski, T., 2017. Comparison of meteorological conditions in Svalbard fjords: Hornsund and Kongsfjorden. *Oceanologia* 59 (4), 413–421, <http://dx.doi.org/10.1016/j.oceano.2017.06.004>.

- Dee, D.P., Uppala, S.M., Simmons, A.J., Berrisford, P., Poli, P., Kobayashi, S., Andrae, U., Balmaseda, M.A., Balsamo, G., Bauer, P., Bechtold, P., Beljaars, A.C.M., van de Berg, L., Bidlot, J., Bormann, N., Delsol, C., Dragani, R., Fuentes, M., Geer, A.J., Haimberger, L., Healy, S.B., Hersbach, H., Hölm, E.V., Isaksen, L., Källberg, P., Köhler, M., Matricardi, M., McNally, A.P., Monge-Sanz, B.M., Morcrette, J.-J., Park, B.-K., Peubey, C., de Rosnay, P., Tavolato, C., Thépaut, J.-N., Vitart, F., 2011. The ERA-Interim reanalysis: configuration and performance of the data assimilation system. *Q. J. R. Meteorol. Soc.* 137 (656), 553–597, <http://dx.doi.org/10.1002/qj.828>.
- Drange, H., Dokken, T., Furevik, T., Gerdes, R., Berger, W. (Eds.), 2005. *The Nordic Seas: An Integrated Perspective Oceanography, Climatology, Biogeochemistry, and Modeling*. Geophysical Monograph Series. American Geophys. Union, Washington, D.C., 365 pp.
- Environmental Modeling Center/Marine Modeling and Analysis Branch, 2016. WW3 hindcast archive [WWW Document], <ftp://polar.ncep.noaa.gov/pub/history/waves>.
- Guedes Soares, C., 1984. Representation of double-peaked sea wave spectra. *Ocean Eng.* 11 (2), 185–207, [http://dx.doi.org/10.1016/0029-8018\(84\)90019-2](http://dx.doi.org/10.1016/0029-8018(84)90019-2).
- Johannessen, O.M., Bengtsson, L., Miles, M.W., Kuzmina, S.I., Semenov, V.A., Alekseev, G.V., Nagurnyi, A.P., Zakharov, V.F., Bobylev, L.P., Pettersson, L.H., Hasselmann, K., Cattle, H.P., 2004. Arctic climate change: observed and modelled temperature and sea-ice variability. *Tellus A* 56 (4), 328–341, <http://dx.doi.org/10.1111/j.1600-0870.2004.00060.x>.
- Kruszewski, G., 2012. *Ice conditions in Hornsund and adjacent waters (Spitsbergen) during winter season 2010–2011*. *Probl. Klimatol. Polar.* 22, 69–82.
- Kumar, S.V., Naseef, M.T., 2015. Performance of ERA-Interim wave data in the nearshore waters around India. *J. Atmos. Oceanic Technol.* 32 (6), 1257–1269, <http://dx.doi.org/10.1175/JTECH-D-14-00153.1>.
- Kushnir, Y., Cardone, V.J., Greenwood, J.G., Cane, M.A., 1997. The recent increase in North Atlantic wave heights. *J. Climate* 10 (8), 2107–2113, [http://dx.doi.org/10.1175/1520-0442\(1997\)010<2107:TRIIINA>2.0.CO;2](http://dx.doi.org/10.1175/1520-0442(1997)010<2107:TRIIINA>2.0.CO;2).
- Kvamstø, N.G., Steinskog, D.J., Stephenson, D.B., Tjøstheim, D.B., 2011. Estimation of trends in extreme melt-season duration at Svalbard. *Int. J. Climatol.* 32 (14), 2227–2239, <http://dx.doi.org/10.1002/joc.3395>.
- Lee, H., 2005. addaxis [WWW Document], <http://www.mathworks.com/matlabcentral/fileexchange/9016-addaxis> (accessed 14.10.16).
- National Center for Environmental Prediction, 2016. Northern Hemisphere Teleconnection Patterns [WWW Document], <http://www.cpc.ncep.noaa.gov/data/teledoc/telecontents.shtml>.
- National Center for Environmental Prediction, 2016. Climate Data Assimilation System Sea Ice Concentrations, January 1, 1979 to Present [WWW Document], <ftp://polar.ncep.noaa.gov/pub/cdas/>.
- Norwegian Meteorological Institute, 2016. Ice Information Portal [WWW Document], <http://polarview.met.no/> (accessed 9.6.16).
- Onarheim, I.H., Smedsrød, L.H., Ingvaldsen, R.B., Nilsen, F., 2014. Loss of sea ice during winter north of Svalbard. *Tellus A* 66 (1), 23933, <http://dx.doi.org/10.3402/tellusa.v66.23933>.
- Osuch, M., Wawrzyniak, T., 2016. Inter- and intra-annual changes in air temperature and precipitation in western Spitsbergen. *Int. J. Climatol.* 37 (7), 3082–3097, <http://dx.doi.org/10.1002/joc.4901>.
- Pereira, D., 2014. Wind Rose [WWW Document], <http://www.mathworks.com/matlabcentral/fileexchange/47248-wind-rose> (accessed 14.10.16).
- Portilla, J., Ocampo-Torres, F.J., Monbaliu, J., 2009. Spectral partitioning and identification of wind sea and swell. *J. Atmos. Ocean. Technol.* 26 (1), 107–122, <http://dx.doi.org/10.1175/2008JTECHO609.1>.
- Przybylak, R., 2003. *The Climate of the Arctic, Atmospheric and Oceanographic Sciences Library*. Kluwer Acad. Publ., Dordrecht, Boston, 270 pp.
- Reistad, M., Breivik, Ø., Haakenstad, H., Aarnes, O.J., Furevik, B.R., Bidlot, J.-R., 2011. A high-resolution hindcast of wind and waves for the North Sea, the Norwegian Sea, and the Barents Sea. *J. Geophys. Res.* 116 (C5), C05019, <http://dx.doi.org/10.1029/2010JC006402>.
- Saloranta, T.M., Haugan, P.M., 2001. Interannual variability in the hydrography of Atlantic water northwest of Svalbard. *J. Geophys. Res.* 106 (C7), 13931–13943, <http://dx.doi.org/10.1029/2000JC000478>.
- Semedo, A., Vettor, R., Breivik, Ø., Sterl, A., Reistad, M., Guedes Soares, C., Lima, D., 2015. The wind sea and swell waves climate in the Nordic seas. *Ocean Dyn.* 65 (2), 223–240, <http://dx.doi.org/10.1007/s10236-014-0788-4>.
- Sessford, E.G., Gøril Bæverford, M., Hormes, A., 2015. Terrestrial processes affecting unlithified coastal erosion disparities in central fjords of Svalbard. *Polar Res.* 34 (1), 24122, <http://dx.doi.org/10.3402/polar.v34.24122>.
- Stopa, J.E., Cheung, K.F., 2014. Intercomparison of wind and wave data from the ECMWF Reanalysis Interim and the NCEP Climate Forecast System Reanalysis. *Ocean Model.* 75, 65–83, <http://dx.doi.org/10.1016/j.ocemod.2013.12.006>.
- Stopa, J.E., Arduin, F., Girard-Arduin, F., 2016. Wave climate in the Arctic 1992–2014: seasonality and trends. *Cryosphere* 10 (4), 1605–1629, <http://dx.doi.org/10.5194/tc-10-1605-2016>.
- Styszynska, A., Buchert, L., 2004. The sea ice cover in Hornsund Fjord and its foreshore (SW Spitsbergen) during winter season 2003/2004. In: Styszynska, A., Marsz, A.A. (Eds.), Polish Polar Studies: 30th International Polar Symposium, Gdynia, 2004. Maritime Univ., Gdynia, 369–376.
- Teena, N.V., Sanil Kumar, V., Sudheesh, K., Sajeev, R., 2012. Statistical analysis on extreme wave height. *Nat. Hazards* 64 (1), 223–236, <http://dx.doi.org/10.1007/s11069-012-0229-y>.
- Thomas, T.J., Dwarakish, G.S., 2015. Numerical wave modelling – a review. *Aquatic Proc.* 4, 443–448, <http://dx.doi.org/10.1016/j.aqpro.2015.02.059>.
- Tolman, H.L., 2014. User Manual and System Documentation of WAVEWATCH III(R) VERSION 4.18 [WWW Document], <http://polar.ncep.noaa.gov/waves/wavewatch/manual.v4.18.pdf> (accessed 9.5.16).
- Tuomi, L., Kahma, K.K., Pettersson, H., 2011. Wave hindcast statistics in the seasonally ice-covered Baltic Sea. *Boreal Environ. Res.* 16 (6), 451–472.
- Wang, X.L., Swail, V.R., 2001. Changes of extreme wave heights in northern hemisphere oceans and related atmospheric circulation regimes. *J. Climate* 14 (10), 2204–2221, [http://dx.doi.org/10.1175/1520-0442\(2001\)014<2204:COEWHI>2.0.CO;2](http://dx.doi.org/10.1175/1520-0442(2001)014<2204:COEWHI>2.0.CO;2).
- Young, I.R., Zieger, S., Babanin, A.V., 2011. Global trends in wind speed and wave height. *Science* 332 (6028), 451–455, <http://dx.doi.org/10.1126/science.1197219>.
- Zacharioudaki, A., Korres, G., Perivoliotis, L., 2015. Wave climate of the Hellenic Seas obtained from a wave hindcast for the period 1960–2001. *Ocean Dyn.* 65 (6), 795–816, <http://dx.doi.org/10.1007/s10236-015-0840-z>.
- Zagórski, P., Rodzik, J., Moskalik, M., Strzelecki, M.C., Lim, M., Błaszczyk, M., Promińska, A., Kruszewski, G., Styszynska, A., Malczewski, A., 2015. Multidecadal (1960–2011) shoreline changes in Isbjørnhamna (Hornsund, Svalbard). *Pol. Polar Res.* 36 (4), 369–390, <http://dx.doi.org/10.1515/popore-2015-0019>.
- Zhao, X., Shen, H.H., Cheng, S., 2015. Modeling ocean wave propagation under sea ice covers. *Acta Mech. Sin. Xuebao* 31 (1), 1–15, <http://dx.doi.org/10.1007/s10409-015-0017-5>.